Actin Cytoskeleton Regulates Stretch-Activated Ca^{2+} Influx in Human Pulmonary Microvascular Endothelial Cells

Satoru Ito[1], Béla Suki[5], Hiroaki Kume[1], Yasushi Numaguchi[2], Masakazu Ishii[2], Mai Iwaki[1], Masashi Kondo[1], Keiji Naruse[4], Yoshinori Hasegawa[1], and Masahiro Sokabe[3,6,7]

[1]Department of Respiratory Medicine, [2]Department of Medical Science of Proteases, and [3]Department of Physiology, Nagoya University Graduate School of Medicine, Nagoya, Japan; [4]Department of Cardiovascular Physiology, Okayama University Graduate School of Medicine, Okayama, Japan; [5]Department of Biomedical Engineering, Boston University, Boston, Massachusetts, [6]ICORP/SORST Cell Mechanosensing, JST, Nagoya; and [7]Department of Molecular Physiology, National Institute for Physiological Sciences, Okazaki, Japan

During high tidal volume mechanical ventilation in patients with acute lung injury (ALI)/acute respiratory distress syndrome (ARDS), regions of the lung are exposed to excessive stretch, causing inflammatory responses and further lung damage. In this study, the effects of mechanical stretch on intracellular Ca^{2+} concentration ($[Ca^{2+}]_i$), which regulates a variety of endothelial properties, were investigated in human pulmonary microvascular endothelial cells (HPMVECs). HPMVECs grown on fibronectin-coated silicon chambers were exposed to uniaxial stretching, using a cell-stretching apparatus. After stretching and subsequent unloading, $[Ca^{2+}]_i$, as measured by fura-2 fluorescence, was transiently increased in a strain amplitude–dependent manner. The elevation of $[Ca^{2+}]_i$ induced by stretch was not evident in the Ca^{2+}-free solution and was blocked by Gd^{3+}, a stretch-activated channel inhibitor, or ruthenium red, a transient receptor potential vanilloid inhibitor. The disruption of actin polymerization with cytochalasin D inhibited the stretch-induced elevation of $[Ca^{2+}]_i$. In contrast, increases in $[Ca^{2+}]_i$ induced by thapsigargin or thrombin were not affected by cytochalasin D. Increased actin polymerization with sphingosine-1-phosphate or jasplakinolide enhanced the stretch-induced elevation of $[Ca^{2+}]_i$. A simple network model of the cytoskeleton was also developed in support of the notion that actin stress fibers are required for efficient force transmission to open stretch-activated Ca^{2+} channels. In conclusion, mechanical stretch activates Ca^{2+} influx via stretch-activated channels which are tightly regulated by the actin cytoskeleton different from other Ca^{2+} influx pathways such as receptor-operated and store-operated Ca^{2+} entries in HPMVECs. These results suggest that abnormal Ca^{2+} homeostasis because of excessive mechanical stretch during mechanical ventilation may play a role in the progression of ALI/ARDS.

Keywords: Ca^{2+} channels; F-actin; mechanotransduction; mechanical stress; stretch-activated channel

CLINICAL RELEVANCE

The lung in mechanically ventilated patients with acute lung injury (ALI) or acute respiratory distress syndrome (ARDS) is exposed to excessive cyclic mechanical stretching, which often causes further damage to the lung, referred to as ventilator-induced lung injury. Here, we demonstrate that uniaxial mechanical stretch induces stretch-activated Ca^{2+} influx different from other Ca^{2+} influx pathways such as receptor-operated and store-operated Ca^{2+} entries in human pulmonary microvascular endothelial cells. Excessive mechanical strain during high tidal ventilation may cause further lung damage via abnormal endothelial Ca^{2+} homeostasis in patients with ALI/ARDS.

The lung in mechanically ventilated patients with acute lung injury (ALI) or acute respiratory distress syndrome (ARDS), a complex and devastating illness, is exposed to excessive cyclic mechanical stretching that often causes further damage to the lung. This damage is refereed to as ventilator-induced lung injury (VILI) (1–3). Hence, lung-protective ventilation with lower tidal volumes to reduce tissue stretch has been proposed in the management of ALI/ARDS (2). A primary target of mechanical stretch in VILI involves microvascular (capillary) endothelial cells (ECs) in the lung (4, 5). Indeed, cellular stress failure and the increased permeability of pulmonary ECs are recognized as major pathophysiologic events associated with VILI (3, 4).

Many functional properties of vascular ECs are dynamically regulated by mechanical forces such as shear stress, pressure, and mechanical stretch, both in physiologic and disease conditions (6). The mechanisms of sensing mechanical forces (mechanosensing) and converting these forces into intracellular biochemical signals (mechanotransduction) are recognized to involve membrane extracellular matrix receptors (e.g., integrins), actin cytoskeleton, and mechanosensitive ion channels (6–8). As in other mammalian cell types, Ca^{2+} influx through Ca^{2+}-permeable stretch-activated (SA) cation channels was found to be one of the second messengers for mechanotransduction in human umbilical vein ECs (HUVECs) and aortic ECs (9–14). Nevertheless, no direct evidence yet exists for an increase in intracellular Ca^{2+} concentration ($[Ca^{2+}]_i$) attributable to mechanical stretch in human pulmonary ECs.

An increase in $[Ca^{2+}]_i$ is essential for a number of important cellular functions, such as NO production, for maintaining normal vascular homeostasis in ECs (15). On the other hand, an excessive elevation of $[Ca^{2+}]_i$ induced by ionomycin or thrombin promotes EC permeability and the formation of edema in the lung (16–18). Parker and colleagues (19) demonstrated that Gd^{3+}, a potent inhibitor of SA channels, prevents the increase in vascular permeability induced by high airway pressure ventilation in isolated rat lungs. Furthermore, both *in vivo* and *ex vivo* studies in rodents showed that an inhibition of transient receptor potential vanilloid (TRPV)-4, a subfamily

(*Received in original form February 25, 2009 and in final form June 22, 2009*)

This work was supported by Grant-in-Aid for Young Scientists A19689017 from the Ministry of Education, Culture, Sports, Science, and Technology of Japan (S.I.), by Grant for Scientific Research on Priority Areas 15,086,270 and Grant for Creative Scientific Research 16GS0308 from MEXT, Japan (M.S.), and National Heart, Lung, and Blood Institute Grant HL-59215 (B.S.).

Correspondence and requests for reprints should be addressed to Satoru Ito, M.D., Ph.D., Department of Respiratory Medicine, Nagoya University Graduate School of Medicine, 65 Tsurumai-cho, Showa-ku, Nagoya 466-8550, Japan. E-mail: itori@med.nagoya-u.ac.jp

Am J Respir Cell Mol Biol Vol 43. pp 26–34, 2010
Originally Published in Press as DOI: 10.1165/rcmb.2009-0073OC on July 31, 2009
Internet address: www.atsjournals.org

of transient receptor potential (TRP) cation channels, reduces lung injury induced by physical forces such as mechanical ventilation (20, 21). These findings suggest that an excessive elevation of $[Ca^{2+}]_i$ in response to physical forces may contribute to the pathogenesis of VILI (22).

This study was designed to determine whether mechanical forces affect intracellular Ca^{2+} homeostasis, and if so, how stretch regulates $[Ca^{2+}]_i$ in human pulmonary microvascular ECs (HPMVECs). We reasoned that if mechanical forces do influence $[Ca^{2+}]_i$, the actin cytoskeleton should play a critical role in regulating the cellular response, because the cytoskeleton is known to be involved in many important cell functions induced by both mechanical and chemical stimuli in pulmonary vascular ECs (4, 23–25). To this end, we used an image-analysis system and a cell-stretching device that allowed us to visualize changes in $[Ca^{2+}]_i$ after mechanical stretching (26). Furthermore, we developed a simple network model of the cytoskeleton to investigate force transmission with the cell. Our results demonstrate that mechanical stretch elevates $[Ca^{2+}]_i$, and that this response is tightly regulated by the actin cytoskeleton in HPMVECs.

MATERIALS AND METHODS

Reagents

Thrombin and nifedipine were obtained from Sigma (St. Louis, MO). Cytochalasin D, jasplakinolide, and thapsigargin were from Calbiochem (La Jolla, CA). Sphingosine-1-phosphate (S1P) was from Biomol (Plymouth Meeting, PA). The $GdCl_3$ was from Wako (Osaka, Japan), the ruthenium red was from Latoxan (Valence, France), and acetoxymethyl ester of fura-2 (fura-2/AM) was obtained from Dojin (Kumamoto, Japan).

Human Pulmonary Microvascular Endothelial Cell Culture

The HPMVECs from multiple donors were obtained from Cambrex (Walkersville, MD). The cells were maintained in culture medium containing 5% FBS, human recombinant epidermal growth factor (1 ng/ml), insulin (10 μg/ml), human recombinant fibroblast growth factor (2 ng/ml), gentamicin (50 μg/ml), and amphotericin B (50 ng/ml) (EGM-2MV; Cambrex) in an environment of 5% CO_2 and 95% air at 37°C. The expression of endothelial markers platelet EC adhesion molecule-1 (CD31) and Tie-2 was confirmed by immunofluorescent staining (data not shown). The HPMVECs were stained with the lectins *Griffonia simplicifolia* and *Helix pomatia*, which recognize microvascular and macrovascular endothelial cells, respectively (27, 28). Staining with FITC-conjugated *Griffonia simplicifolia* but not with FITC-labeled *Helix pomatia* was observed (data not shown).

Application of Uniaxial Stretch

Uniaxial mechanical stretching was applied to the HPMVECs obtained at passages 4–7, using a stretching apparatus (ST-150; Strex, Osaka, Japan) (26). The cells were removed from the dish with 0.01% EDTA-0.02% trypsin, and transferred to a silicon chamber (8 mm long, 8 mm wide, and 3 mm deep) coated with 50 μg/ml human fibronectin (BD Biosciences, Bedford, MA). One end of the chamber was clamped with a fixed metal frame, and the other end was clamped with a movable frame that was connected to a shaft driven by a computer-controlled stepping motor. This apparatus was able to control the amplitude and rate of stretch. The chamber was uniaxially stretched with a strain amplitude between 10 and 30% and at a steady rate of 0.1%/ms. At the desired peak strain, the chamber was held for 3 seconds in the stretched position, and returned to the initial unstretched state at the same rate as during the stretching phase. We confirmed that the bottom of the chamber was stretched uniformly over the area of interest. Cell viability, as examined by morphology and trypan blue exclusion, was not affected by mechanical stretch under these experimental conditions.

Measurement of Intracellular Ca^{2+} Concentrations

The cells (~ 50% confluence) in the silicon chamber were treated with 3 μM fura-2/AM for 25 min at 37°C in normal physiologic solution containing NaCl at 145 mM, KCl at 5 mM, $CaCl_2$ at 2 mM, $MgCl_2$ at 1 mM, glucose at 10 mM, and HEPES at 10 mM (pH 7.40). The nominally Ca^{2+}-free solution was prepared by replacing $CaCl_2$ with $MgCl_2$. After the cells were washed with normal solution, $[Ca^{2+}]_i$ was assessed according to the fluorescence of fura-2, using a fluorescence microscope with a ×20 objective (Fluor20; Nikon, Tokyo, Japan), as described previously (26). Data were analyzed using a digital fluorescence imaging system (Aquacosmos; Hamamatsu Photonics, Hamamatsu, Japan). The excitation wavelengths were set at 340 and 380 nm, and the emission was collected at 510 nm by a photomultiplier. The intensity of fura-2 fluorescence attributable to excitation at 340 nm (F_{340}) and at 380 nm (F_{380}) was measured after subtraction of the background fluorescence, and the ratio of F_{340} to F_{380} (F_{340}/F_{380} ratio) was used as an indicator of the relative level of $[Ca^{2+}]_i$ (26, 29). The experiments were performed at room temperature (25–27°C).

RNA Isolation and RT-PCR

Total cellular RNA was extracted from HPMVECs and human bronchial smooth muscle cells, using a commercial kit (Takara, Otsu, Japan). The RNA was reverse-transcribed to cDNA, using a Superscript III kit (Invitrogen, Carlsbad, CA). The PCR amplification was performed with 35 cycles of 30 seconds at 94°C, 30 seconds at 60°C, and 60 seconds at 72°C. The sequences of forward and reverse specific primers, respectively, were designed as follows: TRPV-2, 5′-CTT CTTCCAGAAGGGCCAAG-3′ and 5′-AGGTGGCTCAGTCCT GAAAA-3′; TRPV-4, 5′-GCCCCACATTGTCAACTACC-3′ and 5′-TCCAGGGAGGAGAGGTCATA-3′; and glyceraldehyde-3-phosphate dehydrogenase (GAPDH), 5′-AACGGATTTGGTCGTATT GG-3′ and 5′-TGAGTCCTTCCACGATACCA-3′ (26). The product sizes for TRPV-2, TRPV-4, and GAPDH were 384 bp, 376 bp, and 498 bp, respectively. Human bronchial smooth muscle cells were used as a positive control for TRPV-2 and TRPV-4 (26).

Immunofluorescent Staining

Confluent HPMVECs grown on glass coverslips (Lab-Tek; Nunc, Rochester, NY) were exposed to experimental conditions, fixed with 4% formaldehyde in PBS for 60 minutes at room temperature, and permeabilized with 0.25% Triton X-100 containing 0.5% BSA for 60 minutes. For the detection of Tie-2 or CD31, cells were incubated with anti-human Tie-2 or CD31 antibody (Santa Cruz Biotechnology, Santa Cruz, CA) for 8 hours, and then with an FITC-conjugated anti-rabbit secondary antibody for 60 minutes at room temperature for immunodetection. The F-actin was stained with fluorochrome-conjugated phalloidin (Alexa488-Phalloidin; Molecular Probes, Eugene, OR) for 60 minutes at room temperature. Nuclei were stained with the DNA binding dye 4,6-diamino-2-phenylindole (DAPI) (Dojin, Kumamoto, Japan). For the lectin-binding assays, cells that had been fixed with 4% formaldehyde in PBS for 60 minutes were incubated with FITC-conjugated *Griffonia simplicifolia* or *Helix pomatia* (Sigma) for 60 minutes at room temperature. The immunofluorescently stained cells were then visualized by fluorescence microscopy and an imaging system (Biozero BZ-8000; Keyence, Osaka, Japan).

Modeling the Cytoskeleton

To examine the possible mechanisms of force transmission within the cell, we developed a simple two-dimensional network model of the actin cytoskeleton, based on a hexagonal lattice of linear springs similar to that introduced in our previous work (30). The network was diluted by removing the spring from the inside, to form a structure similar to a cell. The outer boundary of the network modeled the plasma membrane, whereas a layer of springs just below the boundary represented the peripheral actin network. In addition, two nearly straight sets of springs connecting the top and bottom boundaries were included as a model of stress fibers (Figure 1). Each spring was assigned a spring constant of $K = 1$. The stiffness (K_f) of the springs representing the stress fibers could assume two different values: either 0.01, mimicking actin disruption by cytochalasin D, or 100, mimicking the elasticity of an intact actin stress fiber. In addition to the regular springs, torsional springs, called bond bending, were also included in the model. The torsional spring resists the change in angle between two springs. The larger the bond bending constant b, the more difficult it is

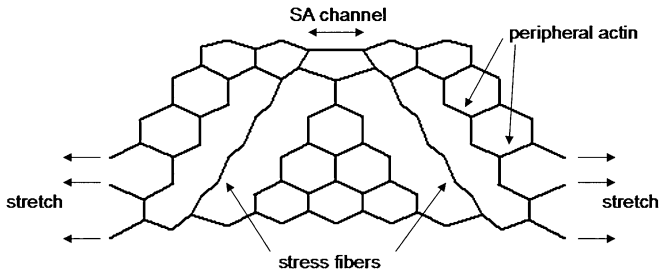

Figure 1. A diluted hexagonal network model of the cell shows peripheral actin, stress fibers, and a stretch-activated channel (*see* text for further explanation).

to change the angle between two springs, and consequently, the stress fiber in the model resists bending. The bond bending also keeps the network stable and inflated. The model was then stretched at the base and the three unconnected side springs (Figure 1) to 20% uniaxial strain in the horizontal direction. The x and y coordinates of the base and the three unconnected side springs were fixed in their position after the stretch, whereas all other springs were allowed to move. The configuration of the network was solved by minimizing the total elastic energy, which included stretching the regular springs, and rotating the torsional springs, using a modified, simulated annealing algorithm (31). Briefly, the local equilibrium position of each node was computed, based on the forces carried by the springs connected to a node. Next, each node was moved in the direction of its equilibrium position with a small amount proportional to the local force, and the total energy E of the network was recalculated. If the change in energy was negative (i.e., $\Delta E < 0$), the configuration was accepted, whereas if $\Delta E > 0$, the configuration was accepted with a probability $P = \exp(-\Delta E/T)$, where T is a control parameter of the algorithm. These steps were then repeated until a convergence criterion was reached ($\Delta E/E < 10^{-7}$). The strain on the two top middle springs (with K = 1) mimicking a single SA channel was then determined for various combinations of the model parameters.

Statistical Analysis

All data were expressed as means ± SD (ANOVA), followed by the Bonferroni test for post hoc analysis, or else an unpaired *t* test was used to evaluate statistical significance. $P < 0.05$ was considered statistically significant.

RESULTS

Mechanical Stretch Increases Intracellular Ca^{2+} Concentration

The HPMVECs cultured on elastic silicon membranes were uniaxially stretched to peak strains of 10%, 20%, or 30%, held for 3 seconds, and returned to their initial unstretched state. Representative cell images of the F_{340}/F_{380} ratio, a measure of $[Ca^{2+}]_i$, before and 3 seconds after the application of 30% stretch, are shown in Figure 2A. A typical time course of changes in the F_{340}/F_{380} ratio of cells in response to sequentially applied, different stretch amplitudes (10–30%) is shown in Figure 2B. After the application of a single uniaxial stretch (20% or 30%) and subsequent unloading, the F_{340}/F_{380} ratio quickly increased and then slowly declined (Figure 2B). The rapid transient spikes in the time course of the response signals during stretching are artifacts (Figure 2B). The increases in F_{340}/F_{380} ratio were significantly strain amplitude-dependent ($n = 12$, $P < 0.001$) (Figure 2C), with no change in F_{340}/F_{380} ratio observed at 10% strain amplitude (Figure 2B and C).

Role of Ca^{2+} Influx via SA Channels in Stretch-Induced Increase of $[Ca^{2+}]_i$

To examine the contribution of Ca^{2+} influx from the extracellular side to the stretch-induced $[Ca^{2+}]_i$ increases in HPMVECs, stretching was applied to the silicon chamber in Ca^{2+}-free solution. A representative time course of the F_{340}/F_{380} ratio, measured in cells in response to 30% strain in the Ca^{2+}-free solution, is shown in Figure 3A. Other than the artifact signal during stretching, no increase in F_{340}/F_{380} ratio was detected in the Ca^{2+}-free solution (Figure 3A). The stretch-induced increase in F_{340}/F_{380} ratio was significantly inhibited in the Ca^{2+}-free solution ($n = 5$, $P < 0.001$) (Figure 3C). When thapsigargin (1 μM), an inhibitor of sarco-endoplasmic reticulum Ca^{2+} ATPase, was applied to the chamber in the Ca^{2+}-free solution, the F_{340}/F_{380} ratio increased gradually because of Ca^{2+} leakage from Ca^{2+} stores in the endoplasmic reticulum (ER) (Figure 3D). These findings suggest that the main pathway for the characteristic stretch-induced $[Ca^{2+}]_i$ increase, as demonstrated by F_{340}/F_{380} ratios, involved the influx of Ca^{2+} from the

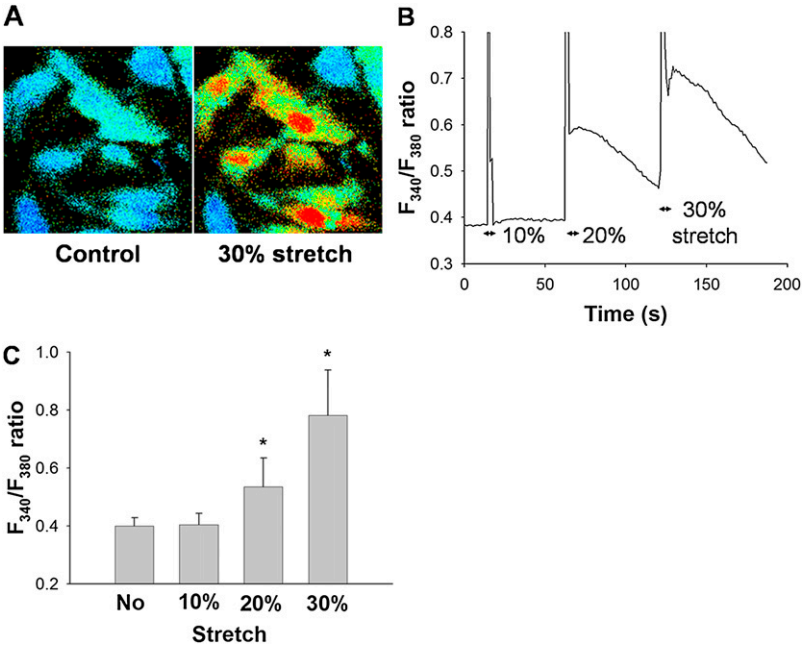

Figure 2. (*A*) Representative images of changes are shown in fura-2 fluorescence signal (F_{340}/F_{380} ratio), an index of intracellular Ca^{2+} concentrations, in the same position before (control, *left*) and after a uniaxial stretch equivalent to 30% peak strain amplitude (*right*). Bright (*red*, *yellow*, and *green*) and dark (*black* and *blue*) colors represent higher and lower F_{340}/F_{380} levels, respectively. (*B*) Representative time courses of F_{340}/F_{380} ratio for 10%, 20%, and 30% uniaxial peak strains. (C) The F_{340}/F_{380} ratio without stretching and in response to 10%, 20%, or 30% strain. Bars represent means ± SD ($n = 5$). *Significantly different from values in unstretched condition ($P <$ 0.001; one-way, repeated-measures ANOVA with Bonferroni test).

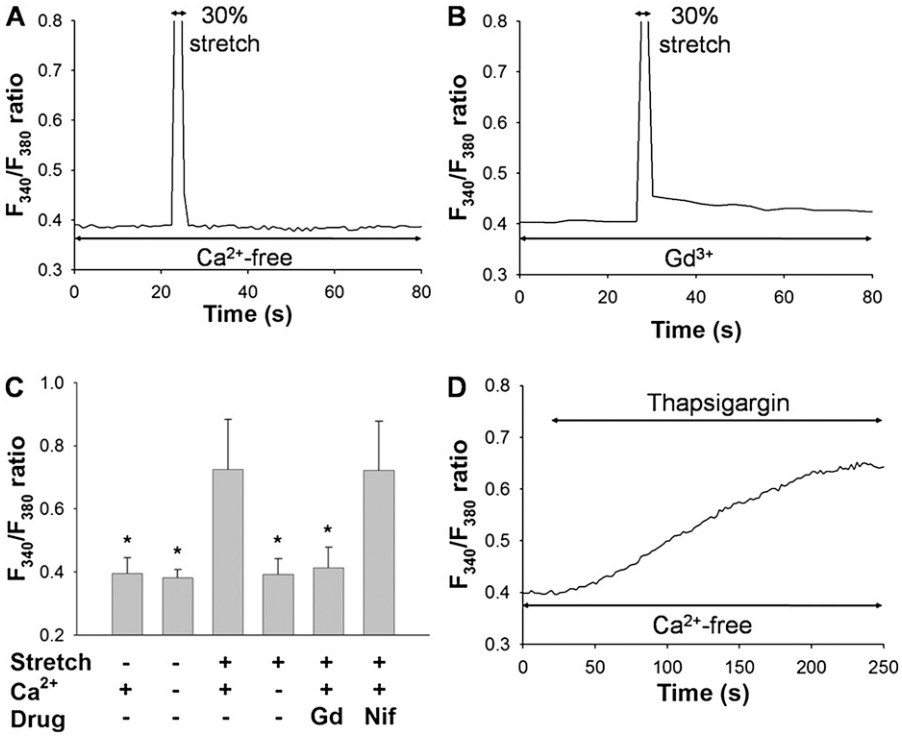

Figure 3. Roles of Ca^{2+} influx from extracellular side in F_{340}/F_{380} signals after a mechanical stretch equivalent to 30% strain. Representative traces of changes in F_{340}/F_{380} ratio in a Ca^{2+}-free solution (*A*) and in the presence of 10 μM Gd^{3+}, a stretch-activated cation channel inhibitor (*B*). (*C*) Effects of extracellular Ca^{2+}, 10 μM Gd^{3+}, or 10 μM nifedipine (*Nif*) on levels of F_{340}/F_{380} ratio in response to 30% mechanical stretch. Extracellular medium contains either 2 mM (normal solution) or 0 mM (Ca^{2+}-free solution) of Ca^{2+}. Bars represent means ± SD ($n = 6$). *Significantly different from values corresponding to stretched condition in normal solution ($P < 0.001$; one-way ANOVA with Bonferroni test). (*D*) Representative trace of F_{340}/F_{380} ratio after application of 1 μM thapsigargin in Ca^{2+}-free solution.

extracellular side, rather than the release of Ca^{2+} from the ER Ca^{2+} stores.

When 30% strain was applied to the chamber in the presence of 10 μM Gd^{3+}, a potent inhibitor of SA channels, the augmentation of the F_{340}/F_{380} ratio elicited by stretch was significantly reduced ($n = 5$, $P < 0.001$) (Figures 3B and 3C). On the other hand, the increase in F_{340}/F_{380} ratio attributable to stretch was not inhibited by 10 μM nifedipine, an inhibitor of the voltage-gated L-type Ca^{2+} channel (Figure 3C), implying that the L-type Ca^{2+} channel is not involved in the stretch-induced Ca^{2+} influx in HPMVECs. The baseline F_{340}/F_{380} ratio was not affected by Gd^{3+} or nifedipine.

Role of TRPV Family Ion Channels in Stretch-Induced Influx of Ca^{2+}

We examined the possible involvement of TRPVs in the stretch-induced increase of $[Ca^{2+}]_i$. An increase of the F_{340}/F_{380} ratio induced by 30% stretch was significantly inhibited by 10 μM ruthenium red, an inhibitor of TRPV subfamily channels ($P < 0.001$) (Figures 4A and 4B). We next investigated whether the mRNAs of TRPV-2 and TRPV-4, both of which are candidates for SA channels, are expressed in HPMVECs, using RT-PCR. The expression of both TRPV-2 and TRPV-4 mRNA was detected in HPMVECs and human bronchial smooth muscle cells (a positive control) (Figure 4C). These results provide evidence that the route of Ca^{2+} entry after a uniaxial stretch is through the TRPV ion channels.

Stretch-Induced Influx of Ca^{2+} Is Mediated by Actin Polymerization

We further investigated whether the increase in $[Ca^{2+}]_i$ induced by mechanical stretch was regulated by the actin cytoskeleton. A representative time course of the F_{340}/F_{380} ratio of the cells pretreated with cytochalasin D (0.1 μM, 15 min), an inhibitor of actin polymerization, in response to 30% strain is shown in Figure 5A. The increase in F_{340}/F_{380} ratio induced by the stretch was almost completely abolished by 0.1 μM cytochalasin D ($n = 4$, $P < 0.001$) (Figures 5A and 5B). On the other hand,

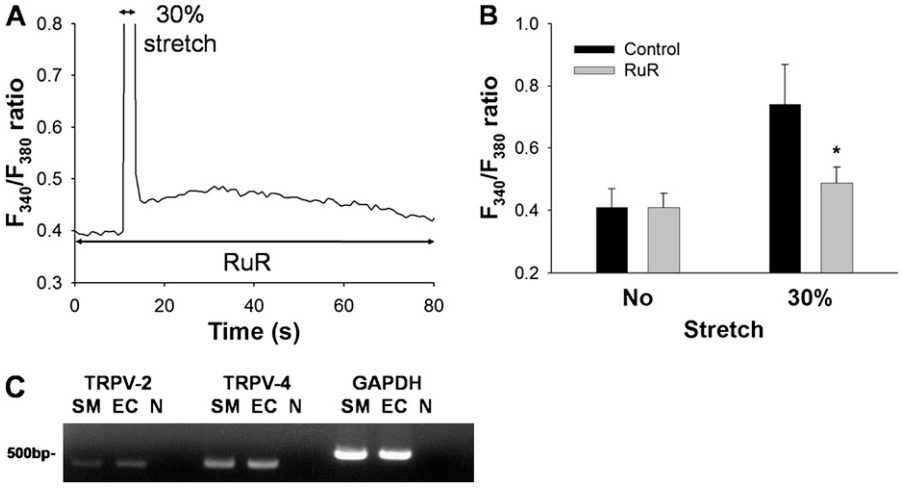

Figure 4. Inhibitory effects of ruthenium red, a TRPV inhibitor, on F_{340}/F_{380} ratio in response to 30% mechanical stretch. (*A*) Representative trace of changes in F_{340}/F_{380} ratio in the presence of 10 μM ruthenium red (*RuR*). (*B*) The F_{340}/F_{380} ratios in response to stretching in the absence (*Control*) or presence of RuR (10 μM). Bars represent means ± SD ($n = 7$). *Significantly different from stretched control values ($P < 0.001$, two-way repeated-measures ANOVA with Bonferroni test). (*C*) Expression of TRPV-2 and TRPV-4 and GAPDH mRNA detected by RT-PCR in HPMVECs (*EC*) and human bronchial smooth muscle cells (*SM*) are shown. *N* indicates a negative control. Product sizes for TRPV-2 and TRPV-4 and GAPDH were 384 bp, 376 bp, and 498 bp, respectively.

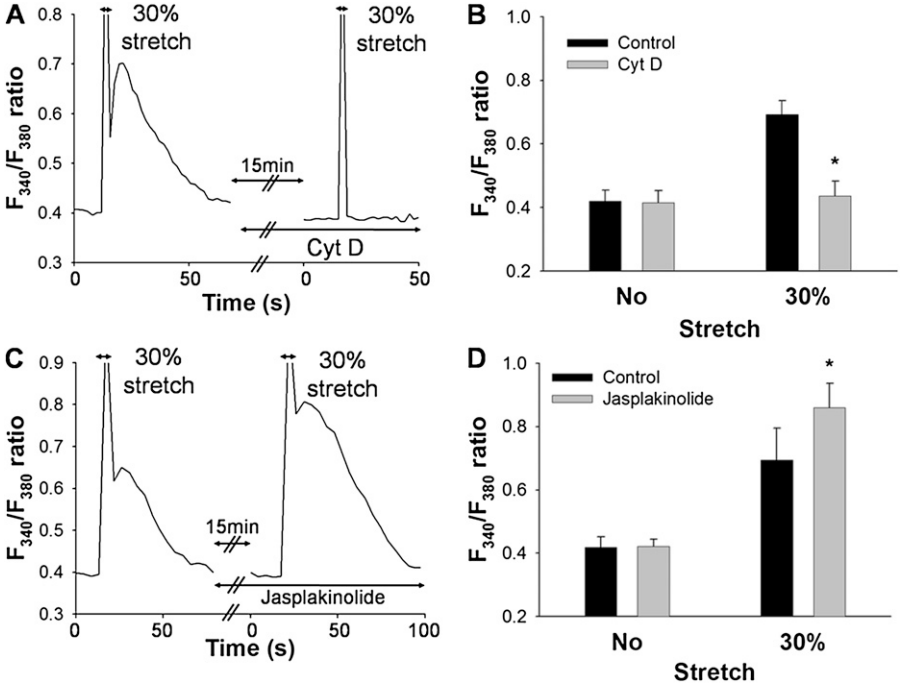

Figure 5. Effects of drugs on actin cytoskeleton, cytochalasin D and jasplakinolide, after a mechanical stretch equivalent to 30% strain. (*A*) Representative trace of changes in F_{340}/F_{380} ratio after mechanical stretching, before and after treatment with 0.1 μM cytochalasin D (*Cyt D*) for 15 min. (*B*) The F_{340}/F_{380} ratios in response to stretching in the absence (*Control*) or presence of 0.1 μM cytochalasin D (*Cyt D*). (*C*) Representative trace of changes in F_{340}/F_{380} ratio before and after treatment with 0.5 μM jasplakinolide for 15 min. (*D*) The F_{340}/F_{380} ratios in response to stretching in the absence (control) or presence of 0.5 μM jasplakinolide. Bars represent means ± SD ($n = 4$). *Significantly different from stretched control values ($P < 0.01$; two-way, repeated-measures ANOVA with Bonferroni test).

preincubation with jasplakinolide (0.5 μM, 15 min), which is known to increase net actin fibers via actin polymerization (32), significantly enhanced the increase in F_{340}/F_{380} ratio induced by stretching ($n = 4$, $P < 0.001$) (Figures 5C and 5D). Neither cytochalasin D nor jasplakinolide treatment directly affected the baseline F_{340}/F_{380} ratio (Figures 5A and 5C).

Next, we examined the effects of sphingolipid S1P, which induces peripheral cytoskeletal rearrangement in pulmonary arterial ECs (25, 33), on the increase of $[Ca^{2+}]_i$ in response to different strain amplitudes (10–30%). Preincubation with S1P (1 μM, 30 min) significantly augmented the stretch-induced increase in F_{340}/F_{380} ratio (Figure 6A). Increases in the F_{340}/F_{380} ratio at 20% and 30% strain were significantly higher in the S1P-treated cells than in control cells ($n = 4$, $P < 0.001$) (Figure 6B). An application of S1P (1 μM) directly induced a transient increase in F_{340}/F_{380} ratio. However, this increase in the F_{340}/F_{380} ratio declined to the initial baseline level within 2 to 5 minutes (Figure 6B). Thus, the baseline F_{340}/F_{380} ratio, when stretching was applied in the presence of S1P, was not significantly different from that of the control sample (Figure 6A).

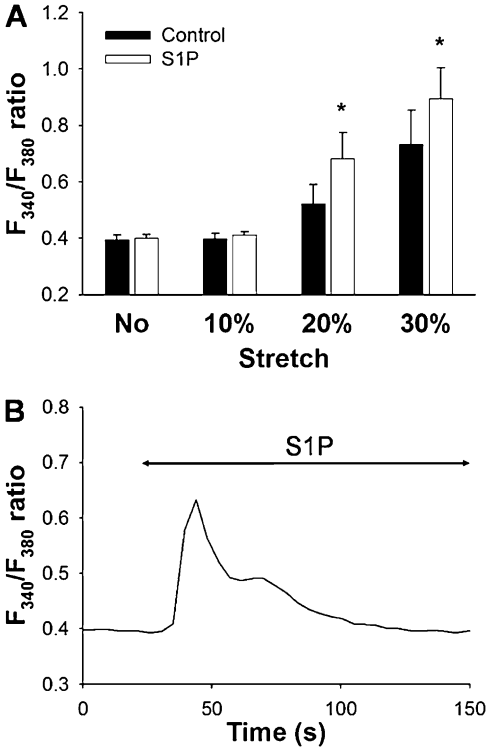

Figure 6. (*A*) Effects of treatment with sphingoshin-1-phosphate (*S1P*) (1 μM, 30 min) on F_{340}/F_{380} ratio after mechanical stretching equivalent to 10%, 20%, or 30% strain. Bars represent means ± SD ($n = 4$). *Significantly different from control values ($P < 0.01$; two-way, repeated-measures ANOVA with Bonferroni test). (*B*) Representative trace of transient increase in F_{340}/F_{380} ratio after application of 1 μM S1P.

Fluorescent Images of F-Actin

Representative images of F-actin polymerization and nuclei stained with Alexa488-phalloidin and DAPI, respectively, are shown in Figure 7. The treatment of cells with 0.1 μM cytochalasin D for 15 minutes reduced actin stress fiber formation (Figure 7B) compared with the normal control sample (Figure 7A). In contrast, the treatment of HPMVECs with S1P (1 μM, 30 min) induced a substantial increase in peripheral F-actin (Figure 7D). Little fluorescence was observed from F-actin stained with Alexa488-phalloidin in cells treated with jasplakinolide (0.5 μM, 15 min) (Figure 7C), because jasplakinolide competitively binds to F-actin at the same binding sites as phalloidin (32, 34).

Effects of Cytochalasin D on Thapsigargin-Induced and Thrombin-Induced Ca^{2+} Signals

Next, we examined the effects of cytochalasin D on the increase of $[Ca^{2+}]_i$ induced by pharmacologic agents such as thapsigargin and thrombin, a G protein–coupled protease-activated receptor agonist. Representative time courses of the F_{340}/F_{380} ratio in response to 1 μM thapsigargin and 10 U/ml thrombin in normal

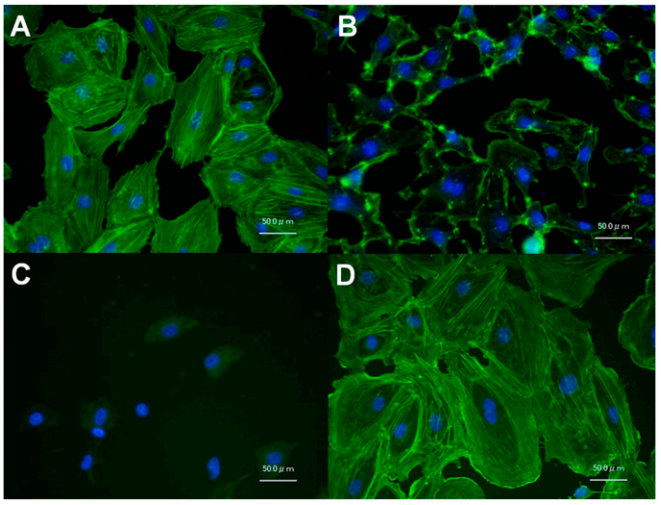

Figure 7. Representative images of control cells (*A*) and cells treated with 0.1 μM cytochalasin D (15 min; *B*), 0.5 μM jasplakinolide (15 min; *C*), and 1 μM S1P (30 min; *D*), on actin polymerization. Nuclei and F-actin were visualized using Alexa488-conjugated phalloidin and DAPI, respectively. Fluorescence from F-actin was negligible in cells treated with jasplakinolide because jasplakinolide competitively binds to F-actin at the same binding sites as phalloidin (*C*).

solution are shown in Figures 8A and 8B, respectively. No stretch-induced increase in F_{340}/F_{380} ratio was evident after treating the cells with cytochalasin D (0.1 μM, 15 min) (Figures 8A and 8C). An application of 1 μM thapsigargin directly increased the F_{340}/F_{380} ratio, which returned to baseline level when extracellular medium was replaced with Ca^{2+}-free solution (Figure 8A). The addition of 2 mM Ca^{2+} back to the extracellular solution quickly increased the F_{340}/F_{380} ratio because of a sustained activation of store-operated Ca^{2+} entry (SOC). Neither the first nor second increase in F_{340}/F_{380} ratio induced by 1 μM thapsigargin was significantly affected by treatment with cytochalasin D (n = 5) (Figure 8B). Similarly, the sustained increase in F_{340}/F_{380} ratio induced by 10 U/ml thrombin was not affected by treatment with 0.1 μM cytochalasin D (n = 5) (Figures 8C and 8D).

Force Transmission in a Network Model of the Cell

A simple two-dimensional network model of a cell based on a diluted hexagonal lattice of linear springs is shown in Figure 1. The results of the simulations are summarized in Table 1. When the bond-bending constant b was 0.1, the stress fibers were unable to stretch the SA channel significantly at the top boundary of the network, independent of the stiffness of the fibers. At the highest b, however, stress fibers with high stiffness produced a 71% strain on the channel, compared with 30% when the fibers were soft. In an additional test, we also eliminated the fibers from the model, and the strain on the SA channel dropped from 30% when soft springs were used to 28% when stress fibers were eliminated. To examine the contribution of peripheral actin, we eliminated nearly half the springs just below the outer layer of the model while K_f was set at 100. The strain on the SA channel decreased from 71% to 61%, suggesting a small contribution of the peripheral network to channel strain. Finally, we repeated the simulations for several different initial network configurations, and found that the results were qualitatively similar.

DISCUSSION

In this study, we provide the first direct evidence that uniaxial stretching induces an increase in $[Ca^{2+}]_i$, which is inhibited both by Ca^{2+}-free solution and by Gd^{3+} in HPMVECs. Moreover, this stretch-induced Ca^{2+} influx is regulated by the actin cytoskeleton, whereas the Ca^{2+} mobilization induced by thapsigargin or thrombin is not affected by an inhibition of the actin polymerization in these cells.

The precise molecular mechanisms by which stretching activates SA channels are not fully understood. Two models have been offered to explain the gating of SA channels both in

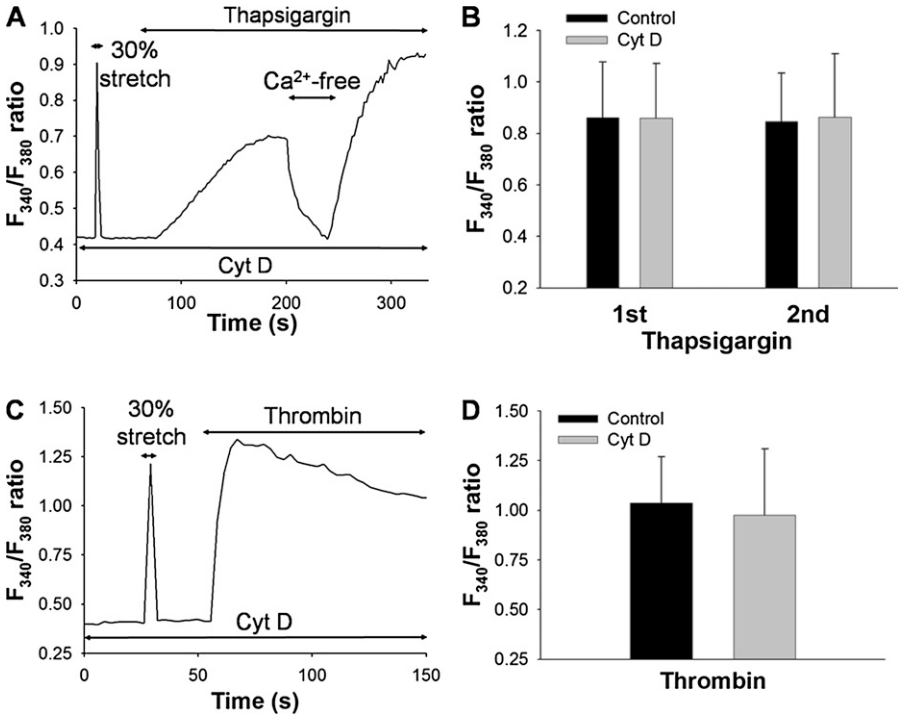

Figure 8. Effects of actin disruption with 0.1 μM cytochalasin D (*Cyt D*) on F_{340}/F_{380} ratio induced by 1 μM thapsigargin or 10 U/ml thrombin. (*A*) Representative trace of F_{340}/F_{380} ratio by stretching to 30% strain, and 1 μM thapsigargin after treatment with 0.1 μM cytochalasin D for 15 min After extracellular solution was changed to Ca^{2+}-free solution for 40 s, 2 mM Ca^{2+} was re-added to the solution. (*B*) Levels of F_{340}/F_{380} ratio in response to thapsigargin before (*1st*) and after (*2nd*) exposing Ca^{2+}-free solution, with (*Control*) or without 0.1 μM cytochalasin D treatment. Bars represent means ± SD (n = 5). (C) Representative trace of F_{340}/F_{380} ratio induced by 30% strain and 10 U/ml thrombin after treatment with 0.1 μM cytochalasin D for 15 min. (*D*) Levels of F_{340}/F_{380} ratio in response to 10 U/ml thrombin with (*Control*) or without 0.1 μM cytochalasin D treatment. Bars represent means ± SD (n = 5).

TABLE 1. STRAIN VALUES ON AN SA CHANNEL IN A NETWORK MODEL OF THE CELL

K_f	b	E_{ch} (%)
0.01	0.1	12
100	0.1	9
0.01	1	27
100	1	32
0.01	10	30
100	10	71

Definition of abbreviations: K_f, stress fiber spring constant; b, bond-bending constant; E_{ch}, strain on SA channel.

prokaryotic and in eukaryotic cells, including mammalian ECs (7, 35). The first model contends that tension in the plasma membrane itself is sufficient to gate the SA channel. In the second model, mechanical forces are transmitted to the SA channel via linkage formed between the extracellular matrix and the cytoskeleton through integrin proteins (36, 37). Our results demonstrate that the SA Ca^{2+} influx was inhibited when the actin network was disrupted with cytochalasin D, whereas the SA Ca^{2+} influx was enhanced by induced peripheral F-actin rearrangement with S1P or jasplakinolide, which are actin-polymerizing agents (Figures 5–7). Thus, our experimental results lend support to the second model: that plasma-membrane tension alone is not sufficient, and the actin cytoskeleton is essential for the activation of SA channels in HPMVECs. Our network model of the cell also supports this conclusion.

The actin cytoskeleton is the major component determining the rheologic properties of single cells (38, 39). Thus, a cell membrane interacting with the underlying cytoskeleton is stiffer than the membrane alone, implying that the cytoskeleton contributes to the force-transmitting ability of the membrane (38, 40). Hayakawa and colleagues (9) demonstrated that the cytoskeleton works as a force-focusing molecular device to activate SA channels in HUVECs. Formigli and colleagues (41, 42) reported that the reorganization of the actin cytoskeleton by S1P enhances SA channel activation, with an increase in cell stiffness measured by atomic force microscopy in C2C12 skeletal muscle cells. In pulmonary arterial ECs, S1P induces the rearrangement of peripheral F-actin with an elevated peripheral elastic modulus, as measured by atomic force microscopy (33). Our findings are consistent with those reports. In contrast, Glogauer and colleagues (43) reported that the influx of Ca^{2+} induced by mechanical stretching is upregulated by actin disruption and downregulated by actin accumulation in human gingival fibroblasts. Thus, the role of the cytoskeleton in SA-channel regulation may be cell type-specific.

The EC functionally possesses several Ca^{2+} influx pathways: specifically, receptor-operated Ca^{2+} entry (ROC) activated by receptor agonists, and SOC, tightly coupled to intracellular Ca^{2+} release from ER Ca^{2+} stores (13, 15, 44). The TRP subfamily TRPC was proposed to form ROC channels in ECs (15). Recent evidence reveals that in ECs, the channel and its regulatory molecule responsible for the SOC are ORAI-1 and STIM-1, respectively (45). Thapsigargin is known to activate SOC via spontaneous Ca^{2+} leakage from the ER in pulmonary ECs (16, 17, 44). Thrombin is considered to activate both ROC via binding to protease-activated receptors, and SOC by stimulating the release of Ca^{2+} from the ER. However, little is known about how these pathways are modulated by mechanical forces. In the present study, although SA Ca^{2+} influx was inhibited by actin disruption with cytochalasin D, the increases in $[Ca^{2+}]_i$ because of the Ca^{2+} influx and release induced by thapsigargin or thrombin were preserved in HPMVECs (Figure 8). Therefore, SA Ca^{2+} influx and other Ca^{2+}-mobilizing pathways, specifically ROC and SOC, are differently regulated by the actin cytoskeleton in HPMVECs.

In the present study, 10 to 30% uniaxial strain was applied to the silicone chamber on which HPMVECs were cultured, using a cell-stretching apparatus. When lung volume is increased to total capacity, the epithelial basement membrane surface area becomes stretched by as much as 40% (46). Although the deformation of the basement membrane during lung inflation is likely more similar to an equi-biaxial condition, the strain pattern to which the ECs are exposed in the microcirculation during high tidal volume ventilation is much more complex. The 40% change in surface area is equivalent to approximately 18% uniaxial strain in one direction. Furthermore, in the lung with ARDS, regional collapse often occurs. As a consequence, open regions can easily receive a tidal ventilation that is equivalent to stretching the region to or above total lung capacity. Because of the heterogeneous nature of regional lung collapse, it is difficult to estimate the strains HPMVECs would experience *in vivo* at peak airway pressures. Nevertheless, the higher strain amplitudes in our *in vitro* study appear to include the magnitudes of strain that could occur during high tidal ventilation *in vivo*. An important limitation of our study involved the use of single stretches, whereas *in vivo*, the lung is exposed to repeated cyclic stretching during ventilation. Future studies should explore the effects of cyclic stretching on Ca^{2+} regulation and functions in pulmonary ECs.

Notably, SA Ca^{2+} influx was only evident when relatively high (20% and 30%) strain amplitudes were applied to cells. In other words, there appears to be a strain threshold between 10 and 20% at which Ca^{2+} influx is suddenly triggered. Moreover, an *ex vivo* study in rats demonstrated that Gd^{3+} prevents the increase in vascular permeability of the lung induced by high airway pressure ventilation (19). Thus, the SA Ca^{2+} channels may have a critical opening stress at which the channel diameter transitions from the closed to the open state, allowing Ca^{2+} influx into the cell. Furthermore, because the Ca^{2+} influx is strain amplitude-dependent (Figure 2C), the channel pore diameter must have an associated elasticity. Because the depolymerization of actin down-regulates the Ca^{2+} influx, the intact actin cytoskeleton may allow mechanical forces to be transmitted nearly instantaneously from the extracellular matrix through focal adhesion cites to various remote focal adhesion sites on the plasma membrane, in concordance with a recent report that locally induced mechanical stimuli rapidly propagate through the prestressed cytoskeleton (47).

The results of our simulations in Table 1 support the notion that to open up SA channels at remote sites of the cell, stress fibers are necessary. These modeling results are also in agreement with recent experimental studies that demonstrated a strong functional association between TRPV-4 channels and F-actin in several cell types (48, 49). Furthermore, our numeric simulations suggest the possibility that peripheral actin in the close neighborhood of the SA channel also contributes to the local transmission of mechanical stimulus, as supported by finding that sphingolipid S1P increased the Ca^{2+} influx, as shown in Figure 6. Interestingly, the remote force transmission in the model was only possible when bond bending was high. In other words, stiff fibers with low bending stiffness (e.g., a strong rope that easily folds) are unable to transmit forces efficiently within the cytoskeleton. In addition to high stiffness, a high bending modulus is also required (e.g., a stiff wire that does not bend easily). This conclusion is in agreement with the finding that the bending stiffness of stress fibers increases strongly with the number of actin filaments within the fiber (50). Nevertheless, several limitations of the model need to be considered. Most importantly, cells *in vivo* undergo cyclic stretching that

was not implemented in the model. If viscous forces are important in force transmission (which has not been studied, to the best of our knowledge), future models will have to implement viscoelastic fibers and a viscous cytoplasm. Second, the fibers were modeled as linear springs. The inclusion of nonlinear fibers would change the effective spring constants, but would likely not alter the qualitative conclusions. However, nonlinearity may produce a threshold phenomenon similar to that observed in the stretch-induced Ca^{2+} entry in Figure 2. Third, the geometry of the model is too simplistic. We used a two-dimensional model with an idealized cytoskeletal structure. Although we would not expect a qualitative change in the model's behavior in three dimensions, a distribution of fiber length and orientation could result in different strain magnitudes on the SA channel. Despite these limitations, this simple model provides supporting evidence for the experimental finding that cytoskeletal stress fibers are essential in the opening of SA channels.

Taken together, Ca^{2+} influx via up-regulated SA channel activity by excessive mechanical stretching in pulmonary microvascular ECs may enhance the VILI in patients with ALI/ARDS. Nevertheless, S1P is known to exert a protective effect on lung injury and endothelial permeability in pulmonary artery ECs by promoting peripheral cytoskeletal rearrangement (24, 25, 51, 52). Sphingosine-1-phosphate may simply strengthen the mechanical integrity of ECs, thus exerting protective effects. Because S1P is a multifunctional sphingolipid with various effects on lung physiology (53), it is still unclear whether or not alterations in intracellular Ca^{2+} homeostasis by S1P play a beneficial role in VILI and ALI/ARDS.

Various mammalian TRP superfamily cation channels were proposed to be mechanosensitive (15, 35). Studies using TRPV-4 knockout mice suggest that TRPV-4 plays a key role in murine models of physical force-induced lung injury (20, 21). Moreover, ruthenium red, an inhibitor of TRPVs, exerts a protective effect in lung injuries induced by physical forces such as mechanical ventilation in mice and rats (20, 21). Indeed, HPMVECs express TRPV-2 and TRPV-4 mRNA, and the increases in $[Ca^{2+}]_i$ induced by mechanical stretching were significantly inhibited by ruthenium red (Figure 4). Thodeti and colleagues demonstrated that TRPV-4 rather than TRPV-2 mediates cyclic stretch-induced Ca^{2+} signaling in bovine adrenal cortex capillary endothelial cells (54). Although the specific TRP genes encoding the putative SA channels responsible for stretch-induced Ca^{2+} influx have not been identified in pulmonary ECs, these findings suggest that TRPVs, and specifically TRPV-4, are responsible for the stretch-induced Ca^{2+} influx in HPMVECs. We also found that 4α-phorbol 12,13-didecanoate (4αPDD), a pharmacologic activator of TRPV-4, causes a sustained increase in $[Ca^{2+}]_i$, which is inhibited by ruthenium red in HPMVECs (data not shown). These findings are consistent with those in rat pulmonary microvascular ECs (55). However, the 4αPDD-induced increase in $[Ca^{2+}]_i$ was not inhibited by cytochalasin D in HPMVECs (data not shown). Thus, although the actin cytoskeleton is necessary for sensing mechanical signals that open the stretch-activated channels (likely TRPV-4), TRPV-4 can be activated directly by its pharmacologic activator, even in the absence of F-actin structure.

In conclusion, we found a novel Ca^{2+} influx pathway, presumably composed of SA cation channels, which is activated by mechanical stretching in HPMVECs. Furthermore, the stretch-activated Ca^{2+} influx was regulated by the actin cytoskeleton. These findings imply that excessive mechanical strain during high tidal ventilation may cause further lung damage via abnormal endothelial Ca^{2+} homeostasis in patients with ALI/ARDS.

Conflict of Interest Statement: K.N. has served on the STREX Advisory Board for up to $1,000. He has received a grant from MENICON for $1,001–$5,000, and a sponsored grant from the National Institutes of Health for $5,001–$10,000. He has a patent pending with STREX for a stretch machine, and owns stock in the amount of $10,001–$50,000. None of the other authors has a financial relationship with a commercial entity that has an interest in the subject of this manuscript.

Acknowledgments: The authors thank Dr. Dimitrije Stamenović, Department of Biomedical Engineering, Boston University, for helpful discussions about network modeling.

References

1. Dos Santos CC, Slutsky AS. The contribution of biophysical lung injury to the development of biotrauma. *Annu Rev Physiol* 2006;68:585–618.
2. ARDS Network. Ventilation with lower tidal volumes as compared with traditional tidal volumes for acute lung injury and the ARDS. *N Engl J Med* 2000;342:1301–1308.
3. Uhlig S, Uhlig U. Pharmacological interventions in ventilator-induced lung injury. *Trends Pharmacol Sci* 2004;25:592–600.
4. Vlahakis NE, Hubmayr RD. Cellular stress failure in ventilator-injured lungs. *Am J Respir Crit Care Med* 2005;171:1328–1342.
5. Marini JJ, Hotchkiss JR, Broccard AF. Bench-to-bedside review: microvascular and airspace linkage in ventilator-induced lung injury. *Crit Care* 2003;7:435–444.
6. Chien S. Mechanotransduction and endothelial cell homeostasis: the wisdom of the cell. *Am J Physiol Heart Circ Physiol* 2007;292:H1209–H1224.
7. Hamill OP, Martinac B. Molecular basis of mechanotransduction in living cells. *Physiol Rev* 2001;81:685–740.
8. Morris CE. Mechanosensitive ion channels. *J Membr Biol* 1990;113:93–107.
9. Hayakawa K, Tatsumi H, Sokabe M. Actin stress fibers transmit and focus force to activate mechanosensitive channels. *J Cell Sci* 2008;121:496–503.
10. Lansman JB, Hallam TJ, Rink TJ. Single stretch-activated ion channels in vascular endothelial cells as mechanotransducers? *Nature* 1987;325:811–813.
11. Naruse K, Yamada T, Sokabe M. Involvement of SA channels in orienting response of cultured endothelial cells to cyclic stretch. *Am J Physiol Heart Circ Physiol* 1998;274:H1532–H1538.
12. Naruse K, Sokabe M. Involvement of stretch-activated ion channels in Ca^{2+} mobilization to mechanical stretch in endothelial cells. *Am J Physiol Cell Physiol* 1993;264:C1037–C1044.
13. Nilius B, Droogmans G. Ion channels and their functional role in vascular endothelium. *Physiol Rev* 2001;81:1415–1459.
14. Oike M, Droogmans G, Nilius B. Mechanosensitive Ca^{2+} transients in endothelial cells from human umbilical vein. *Proc Natl Acad Sci USA* 1994;91:2940–2944.
15. Yao X, Garland CJ. Recent developments in vascular endothelial cell transient receptor potential channels. *Circ Res* 2005;97:853–863.
16. Garcia JG, Schaphorst KL, Shi S, Verin AD, Hart CM, Callahan KS, Patterson CE. Mechanisms of ionomycin-induced endothelial cell barrier dysfunction. *Am J Physiol Lung Cell Mol Physiol* 1997;273:L172–L184.
17. Mehta D, Malik AB. Signaling mechanisms regulating endothelial permeability. *Physiol Rev* 2006;86:279–367.
18. Moore TM, Chetham PM, Kelly JJ, Li M, Stevens T. Signal transduction and regulation of lung endothelial cell permeability: interaction between calcium and cAMP. *Am J Physiol Lung Cell Mol Physiol* 1998;275:L203–L222.
19. Parker JC, Ivey CL, Tucker JA. Gadolinium prevents high airway pressure-induced permeability increases in isolated rat lungs. *J Appl Physiol* 1998;84:1113–1118.
20. Alvarez DF, King JA, Weber D, Addison E, Liedtke W, Townsley MI. Transient receptor potential vanilloid 4-mediated disruption of the alveolar septal barrier. *Circ Res* 2006;99:988–995.
21. Hamanaka K, Jian MY, Weber DS, Alvarez DF, Townsley MI, Al-Mehdi AB, King JA, Liedtke W, Parker JC. TRPV4 initiates the acute calcium-dependent permeability increase during ventilator-induced lung injury in isolated mouse lungs. *Am J Physiol Lung Cell Mol Physiol* 2007;293:L923–L932.
22. Kuebler WM, Ying X, Singh B, Issekutz AC, Bhattacharya J. Pressure is proinflammatory in lung venular capillaries. *J Clin Invest* 1999;104:494–502.
23. Birukov KG, Jacobson JR, Flores AA, Ye SQ, Birukova AA, Verin AD, Garcia JG. Magnitude-dependent regulation of pulmonary endothelial

cell barrier function by cyclic stretch. *Am J Physiol Lung Cell Mol Physiol* 2003;285:L785–L797.
24. Dudek SM, Garcia JG. Cytoskeletal regulation of pulmonary vascular permeability. *J Appl Physiol* 2001;91:1487–1500.
25. Garcia JG, Liu F, Verin AD, Birukova A, Dechert MA, Gerthoffer WT, Bamberg JR, English D. Sphingosine 1-phosphate promotes endothelial cell barrier integrity by EDG-dependent cytoskeletal rearrangement. *J Clin Invest* 2001;108:689–701.
26. Ito S, Kume H, Naruse K, Kondo M, Takeda N, Iwata S, Hasegawa Y, Sokabe M. A novel Ca^{2+} influx pathway activated by mechanical stretch in human airway smooth muscle cells. *Am J Respir Cell Mol Biol* 2008;38:407–413.
27. King J, Hamil T, Creighton J, Wu S, Bhat P, McDonald F, Stevens T. Structural and functional characteristics of lung macro- and microvascular endothelial cell phenotypes. *Microvasc Res* 2004;67:139–151.
28. Alvarez DF, Huang L, King JA, ElZarrad MK, Yoder MC, Stevens T. Lung microvascular endothelium is enriched with progenitor cells that exhibit vasculogenic capacity. *Am J Physiol Lung Cell Mol Physiol* 2008;294:L419–L430.
29. Ito S, Kume H, Yamaki K, Katoh H, Honjo H, Kodama I, Hayashi H. Regulation of capacitative and non-capacitative receptor-operated Ca^{2+} entry by Rho-kinase in tracheal smooth muscle. *Am J Respir Cell Mol Biol* 2002;26:491–498.
30. Ito S, Majumdar A, Kume H, Shimokata K, Naruse K, Lutchen KR, Stamenović D, Suki B. Viscoelastic and dynamic nonlinear properties of airway smooth muscle tissue: roles of mechanical force and the cytoskeleton. *Am J Physiol Lung Cell Mol Physiol* 2006;290:L1227–L1237.
31. Cavalcante FS, Ito S, Brewer K, Sakai H, Alencar AM, Almeida MP, Andrade JS Jr, Majumdar A, Ingenito EP, Suki B. Mechanical interactions between collagen and proteoglycans: implications for the stability of lung tissue. *J Appl Physiol* 2005;98:672–679.
32. Bubb MR, Senderowicz AM, Sausville EA, Duncan KL, Korn ED. Jasplakinolide, a cytotoxic natural product, induces actin polymerization and competitively inhibits the binding of phalloidin to F-actin. *J Biol Chem* 1994;27:14869–14871.
33. Arce FT, Whitlock JL, Birukova AA, Birukov KG, Arnsdorf MF, Lal R, Garcia JG, Dudek SM. Regulation of the micromechanical properties of pulmonary endothelium by S1P and thrombin: role of cortactin. *Biophys J* 2008;95:886–894.
34. Waschke J, Curry FE, Adamson RH, Drenckhahn D. Regulation of actin dynamics is critical for endothelial barrier functions. *Am J Physiol Heart Circ Physiol* 2005;288:H1296–H1305.
35. Maroto R, Raso A, Wood TG, Kurosky A, Martinac B, Hamill OP. TRPC1 forms the stretch-activated cation channel in vertebrate cells. *Nat Cell Biol* 2005;7:179–185.
36. Sokabe M, Sachs F, Jing Z. Quantitative video microscopy of patch clamped membranes, stress, strain, capacitance and stretch channel activation. *Biophys J* 1991;59:722–728.
37. Zhang Y, Gao F, Popov VL, Wen JW, Hamill OP. Mechanically gated channel activity in cytoskeleton-deficient plasma membrane blebs and vesicles from *Xenopus* oocytes. *J Physiol* 2000;523:117–130.
38. Hu S, Chen J, Fabry B, Numaguchi Y, Gouldstone A, Ingber DE, Fredberg JJ, Butler JP, Wang N. Intracellular stress tomography reveals stress focusing and structural anisotropy in cytoskeleton of living cells. *Am J Physiol Cell Physiol* 2003;285:C1082–C1090.
39. Wang N, Naruse K, Stamenović D, Fredberg JJ, Mijailovich SM, Tolić-Nørrelykke IM, Polte T, Mannix R, Ingber DE. Mechanical behavior in living cells consistent with the tensegrity model. *Proc Natl Acad Sci USA* 2001;98:7765–7770.
40. Byfield FJ, Aranda-Espinoza H, Romanenko VG, Rothblat GH, Levitan I. Cholesterol depletion increases membrane stiffness of aortic endothelial cells. *Biophys J* 2004;87:3336–3343.
41. Formigli L, Meacci E, Sassoli C, Chellini F, Giannini R, Quercioli F, Tiribilli B, Squecco R, Bruni P, Francini F, *et al.* Sphingosine 1-phosphate induces cytoskeletal reorganization in C2C12 myoblasts: physiological relevance for stress fibres in the modulation of ion current through stretch-activated channels. *J Cell Sci* 2005;118:1161–1171.
42. Sbrana F, Sassoli C, Meacci E, Nosi D, Squecco R, Paternostro F, Tiribilli B, Zecchi-Orlandini S, Francini F, Formigli L. Role for stress fiber contraction in surface tension development and stretch-activated channel regulation in C2C12 myoblasts. *Am J Physiol Cell Physiol* 2008;295:C160–C172.
43. Glogauer M, Ferrier J, McCulloch CA. Magnetic fields applied to collagen-coated ferric oxide beads induce stretch-activated Ca^{2+} flux in fibroblasts. *Am J Physiol Cell Physiol* 1995;269:C1093–C1104.
44. Wu S, Cioffi EA, Alvarez D, Sayner SL, Chen H, Cioffi DL, King J, Creighton JR, Townsley M, Goodman SR, *et al.* Essential role of a Ca^{2+}-selective, store-operated current (ISOC) in endothelial cell permeability: determinants of the vascular leak site. *Circ Res* 2005;96:856–863.
45. Abdullaev IF, Bisaillon JM, Potier M, Gonzalez JC, Motiani RK, Trebak M. STIM1 and ORAI1 mediate CRAC currents and store-operated calcium entry important for endothelial cell proliferation. *Circ Res* 2008;103:1289–1299.
46. Tschumperlin DJ, Margulies SS. Alveolar epithelial surface area-volume relationship in isolated rat lungs. *J Appl Physiol* 1999;86:2026–2033.
47. Na S, Collin O, Chowdhury F, Tay B, Ouyang M, Wang Y, Wang N. Rapid signal transduction in living cells is a unique feature of mechanotransduction. *Proc Natl Acad Sci USA* 2008;105:6626–6631.
48. Becker D, Bereiter-Hahn J, Jendrach M. Functional interaction of the cation channel transient receptor potential vanilloid 4 (TRPV4) and actin in volume regulation. *Eur J Cell Biol* 2009;88:141–152.
49. Ramadass R, Becker D, Jendrach M, Bereiter-Hahn J. Spectrally and spatially resolved fluorescence lifetime imaging in living cells: TRPV4-microfilament interactions. *Arch Biochem Biophys* 2007;463:27–36.
50. Bathe M, Heussinger C, Claessens MM, Bausch AR, Frey E. Cytoskeletal bundle mechanics. *Biophys J* 2008;94:2955–2964.
51. Peng X, Hassoun PM, Sammani S, McVerry BJ, Burne MJ, Rabb H, Pearse D, Tuder RM, Garcia JG. Protective effects of sphingosine 1-phosphate in murine endotoxin-induced inflammatory lung injury. *Am J Respir Crit Care Med* 2004;169:1245–1251.
52. Tauseef M, Kini V, Knezevic N, Brannan M, Ramchandaran R, Fyrst H, Saba J, Vogel SM, Malik AB, Mehta D. Activation of sphingosine kinase-1 reverses the increase in lung vascular permeability through sphingosine-1-phosphate receptor signaling in endothelial cells. *Circ Res* 2008;103:1164–1172.
53. Uhlig S, Gulbins E. Sphingolipids in the lungs. *Am J Respir Crit Care Med* 2008;178:1100–1114.
54. Thodeti CK, Matthews B, Ravi A, Mammoto A, Ghosh K, Bracha AL, Ingber DE. TRPV4 channels mediate cyclic strain-induced endothelial cell reorientation through integrin-to-integrin signaling. *Circ Res* 2009;104:1123–1130.
55. Yin J, Hoffmann J, Kaestle SM, Neye N, Wang L, Baeurle J, Liedtke W, Wu S, Kuppe H, Pries AR, *et al.* Negative-feedback loop attenuates hydrostatic lung edema via a cGMP-dependent regulation of transient receptor potential vanilloid 4. *Circ Res* 2008;102:966–974.